The Atmospheric Response to Realistic Reduced Summer Arctic Sea Ice Anomalies

Uma S. Bhatt,[1] Michael A. Alexander,[2] Clara Deser,[3] John E. Walsh,[4] Jack S. Miller,[5] Michael S. Timlin,[6] James Scott,[2] and Robert A. Tomas[3]

The impact of reduced Arctic summer sea ice on the atmosphere is investigated by forcing an atmospheric general circulation model, the Community Climate Model (CCM 3.6), with observed sea ice conditions during 1995, a low-ice year. The 51 experiments, which spanned April to October of 1995, were initiated with different states from a control simulation. The 55-year control was integrated using a repeating climatological seasonal cycle of sea ice. The response was obtained from the mean difference between the experiment and control simulations. The strongest response was found during the month of August where the Arctic displays a weak local thermal response, with warmer surface air temperatures and lower sea level pressure (SLP). However, there is a significant remote response over the North Pacific characterized by an equivalent barotropic (anomalies are collocated with height and increase in magnitude) structure, with anomalous high SLP collocated with a ridge in the upper troposphere. The ice anomalies force an increase (decrease) in precipitation north of (along) the North Pacific storm track. A linear baroclinic model forced with the transient eddy vorticity fluxes, transient eddy heat fluxes, and diabatic heating separately demonstrated that transient eddy vorticity fluxes are key to maintaining the anomalous high over the North Pacific. The model's sensitivity to separately imposed ice anomalies in the Kara, Laptev–East Siberian, or Beaufort seas includes SLP, geopotential height, and precipitation changes that are similar to but weaker than the response to the full sea ice anomaly.

[1]Geophysical Institute, Department of Atmospheric Sciences, University of Alaska Fairbanks, Fairbanks, Alaska, USA.

[2]NOAA Earth System Research Laboratory, Boulder, Colorado, USA.

[3]National Center for Atmospheric Research, Boulder, Colorado, USA.

[4]International Arctic Research Center, University of Alaska Fairbanks, Fairbanks, Alaska, USA.

[5]ARSC, University of Alaska Fairbanks, Fairbanks, Alaska, USA.

[6]Department of Atmospheric Sciences, University of Illinois at Urbana-Champaign, Urbana, Illinois, USA.

Arctic Sea Ice Decline: Observations, Projections, Mechanisms, and Implications
Geophysical Monograph Series 180

10.1029/180GM08

1. INTRODUCTION

Summer sea ice in the Arctic decreased at a rate of 4–6% per decade [*Deser et al.*, 2000] through the 1990s, and the melt rate has accelerated to 10% per decade [*Stroeve et al.*, 2007; National Snow and Ice Data Center, press release, 1 October 2007, available at nsidc.org/news/press/2007_seaiceminimum/20071001_pressrelease.html) in the 2000s. In the 1990s the melting of Arctic ice was consistent with the positive phase of the North Atlantic Oscillation (NAO), which is characterized by enhanced storminess and warm moist air penetration into the Arctic. The NAO has approached more neutral values since 2000, yet the ice melt has accelerated. The observed influx of plugs of warm Atlantic layer water into the Arctic provides one likely mechanism

for the continued ice melt [*Polyakov et al.*, 2005], and recent work shows that heat from the Atlantic layer can penetrate through the halocline into the upper ocean [*Walsh et al.*, 2007]. *Maslanik et al.* [2007] demonstrate that even though the NAO is in the negative phase, the net local atmospheric circulation in the Arctic is consistent with continued ice reduction. Another contributor that could hasten ice retreat in summer is enhanced moisture in the Arctic leading to increased downward longwave fluxes [*Francis and Hunter*, 2006]. Circulation trends since 1979 were found to be weak by *Deser and Teng* [this volume], consistent with the view that multiple mechanisms have led to recent ice declines. The summer sea ice is expected to continue its decline based on the recently documented decreases in winter ice [*Comiso*, 2008] and the warm Atlantic water headed for the Arctic that is being tracked by various ocean observing programs [*Polyakov et al.*, 2007]. In a warmer climate large decreases in summer sea ice may become more common, and while the ice anomalies initially result from both atmospheric and oceanic forcing, we hypothesize that they can, in turn, markedly alter the air-sea exchanges of heat and moisture to subsequently influence the large-scale climate.

The summer warming and sea ice reductions are correlated with cold season circulation anomalies [*Wallace et al.*, 1996; *Rigor et al.*, 2002; *Maslanik et al.*, 2007], which lead to changes in low-level horizontal temperature advection. For example, reduced summer sea ice in the Barents-Kara-Laptev seas is associated with anomalously low pressure centered in the Arctic the preceding spring (April–June) [*Deser et al.*, 2000]. The general tendency toward lower pressure in the Arctic [*Walsh et al.*, 1996] from 1960 to 2000 is consistent with enhanced penetration of storms into the Arctic. There has been an increase of warm season cyclone count and intensity in the Arctic (north of 60°N) since late 1950s [*Serreze et al.*, 1997; *Zhang et al.*, 2004]. *Maslanik et al.* [1996] find an increase of cyclone activity over the central Arctic Ocean, which advects warm southerly winds into the Laptev and East Siberian seas as well as transports ice away from the coast. Ice that is particularly thin as a result of wintertime circulation patterns can be easily broken down and transported because of summer storms, further reducing ice area/concentration.

When high-albedo ice is replaced by low-albedo ocean, there is significantly more net solar flux at the surface, increasing the heat stored in the upper layer of the ocean. This heat stored during the summer can then slow the freezeup the following winter as well as melt ice at the ice/ocean interface. There is still a reasonably strong correlation (+0.6) between the time series of EOF1 of sea ice concentration during the summer and that of the following winter [*Deser et al.*, 2000]. By August the sea surface temperature (SST) can warm in the marginal seas by several degrees [*Steele et al.*, 2008] when ice extent is low. Fluxes of sensible and latent heat into the atmosphere increase with a warmer ocean, which, we hypothesize, could exert some influence back on the atmosphere.

Climate models are ideal tools for understanding the influence of sea ice on the atmosphere because in the observations, climate anomalies are dominated by the atmospheric forcing of the ice. *Singarayer et al.* [2006] ran the Hadley Centre Atmospheric Model (HadAM3) with climatological SSTs and observed sea ice concentrations from 1978 to 2000 to investigate the impact of sea ice on the atmospheric circulation. The model surface air temperature (SAT) response to ice forcing most closely matches the observed SAT variability over the 1993–1995 period [see *Singarayer et al.*, 2006, Figure 4a]. This suggests that sea ice forcing played a more important role than SST (note that this simulation used climatological SSTs) in shaping the SAT anomalies. The observed sea ice anomalies display large interannual variability in the mid-1990s and reached a low for the decade in 1995. *Singarayer et al.* [2006] argue that the ice anomalies were likely large enough that sea ice forcing dominated the atmospheric response. The SAT response during summer strengthened and become statistically significant when observed above-normal SSTs replace climatological values. *Sewall* [2005] investigated the response to reduced Arctic sea ice in the Community Climate System Model, version 3 (CCSM3) plus a suite of coupled Intergovernmental Panel on Climate Change Fourth Assessment simulations and found a robust pattern of reduced wintertime precipitation for the western United States by ~30%.

Magnusdottir et al. [2004] and *Deser et al.* [2004] investigated the response to sea ice and SST anomalies during winter in the North Atlantic using CCM3. The ice anomaly pattern corresponds to an enhanced observed trend with ice reductions (increases) east (west) of Greenland. *Magnusdottir et al.* [2004] found a significant model circulation response to sea ice that resembled the negative phase of the North Atlantic Oscillation, which is opposite of the atmospheric pattern that forced the observed sea ice trend, suggesting that sea ice has a negative feedback on the atmosphere. There is growing evidence that a model's internal variability influences its forced response. To investigate this further, *Deser et al.* [2004] decomposed the atmospheric response to sea ice into the part that projects on the leading mode of model variability and the residual from this projection. The leading mode has an equivalent barotropic vertical structure and resembles the NAO, while the residual is baroclinic. A subsequent study by *Deser et al.* [2007] examines the transient response to wintertime sea ice anomalies in the North Atlantic. They analyzed the general circulation model (GCM) out-

put using a linear baroclinic model (LBM) to show that the initial local response is baroclinic and forced by the diabatic heating anomalies associated with surface heat fluxes resulting from reduced sea ice area. The equilibrium response is large scale in extent, barotropic, and primarily maintained by the transient eddy vorticity fluxes. *Peng and Whittaker* [1999] elucidated this eddy-driven mechanism to describe the atmospheric response to midlatitude SSTs in an idealized GCM, which can be applied to surface changes resulting from decreased sea ice. These studies show that the atmosphere responds to surface boundary conditions in ways that can influence the storm track.

Alexander et al. [2004] forced CCM3 with realistic sea ice conditions, characterized by negative (positive) ice extent anomalies east (west) of Greenland, from 1982 to 1983 that had a similar pattern but with a smaller ice area than the anomalies from *Magnusdottir et al.* [2004] and *Deser et al.* [2004]. The pattern of response is similar in the three studies, with positive (negative) height anomalies in the Arctic (midlatitudes). A comparison of ice area to the strength of 500-hPa response reveals a linearly increasing relationship [see *Alexander et al.*, 2004, Figure 9].

Alexander et al. [2004] also examined the response to ice anomalies in the North Pacific and found that the atmospheric response suggested a positive feedback of the ice on the atmosphere. The different atmospheric responses to ice in the North Atlantic and North Pacific may arise from the position of the storm track relative to the ice edge. In the North Atlantic the ice edge is in the vicinity of the storm track, whereas in the North Pacific the ice edge is well north of the storm track. A thorough discussion of additional studies of the response to winter sea ice is presented by *Alexander et al.* [2004].

Numerous GCM simulations have investigated the impact of winter sea ice on the atmosphere but few have examined the atmospheric response to sea surface temperature or sea ice during the summer months. Several studies find the response during summer to be much weaker than winter and focus their analysis on winter [*Parkinson et al.*, 2001; *Singarayer et al.*, 2006]. *Raymo et al.* [1990] reduced the ice to paleoclimatic conditions throughout the year that reached an ice-free Arctic during the month of September. During June, July, and August (JJA) they found a 3°K warming over Greenland and an overall warming over the polar region. They found no significant differences in sea level pressure, evaporation/precipitation ratios, or cloudiness in the North Atlantic.

This study employs CCM3 to investigate the atmospheric response to reduced realistic summer sea ice in the Arctic from the summer of 1995, which had the lowest June–September ice area (based on both extent and concentration) with the exception of the summer of 2007 (Figure 1). Note that the sea ice minimum in September has been close to or well below the 1995 levels since 2002 [*Stroeve et al.*, 2008]. In addition to using realistic sea ice extents and concentrations in the Arctic, the other unique features of our study

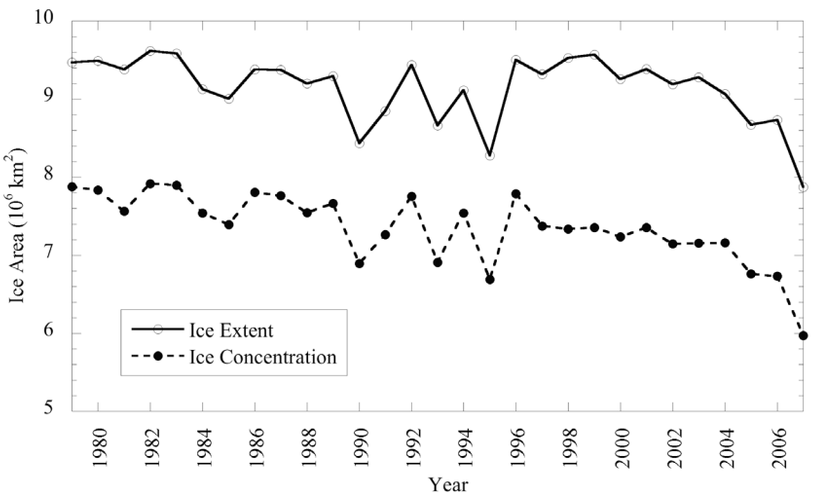

Figure 1. Observed Arctic-wide ice cover (multiplied by 10^6 km^2) based on ice extent (solid line) and concentration (dashed line) during summer (June–September) over the period 1979–2007 in the HadISST1 1° × 1° data set. Ice is defined to extend over a grid square when the ice concentration is 15% or greater. The summer of 1995 had the overall minimum June–September ice extent with the exception of 2007, which was significantly lower.

include the summer focus and the use of a large number (51) of ensemble members for each set of experiments to enhance the signal-to-noise ratio. We chose to employ CCM3 for this study to facilitate a comparison with winter sea ice forcing studies that used the same model [*Alexander et al.*, 2004; *Deser et al.*, 2004; *Magnusdottir et al.*, 2004]. In addition, a suite of further experiments is conducted to investigate the sensitivity of the model to the location of the ice anomaly and a LBM is used to diagnose the forcing to assist in the interpretation of the results.

Some key questions that we address in this study are the following:

- Does the Northern Hemisphere atmosphere respond to realistic summertime Arctic sea ice anomalies? Is there a remote response as well as a local response? How does the response during summer differ from winter?
- Is the atmospheric response sensitive to the placement (latitude/longitude) of the summer Arctic sea ice anomalies?
- How does the response to sea ice extent compare with that to concentration?
- Does the atmospheric response have any implications for feedback mechanisms?

The model experiments are described in section 2, and the results are discussed in section 3. The summary and a discussion of mechanisms are presented in section 4.

2. MODEL EXPERIMENTS

2.1. Boundary Conditions and Experiment Design

Boundary conditions for the simulations are from the Hadley Centre sea ice concentration and sea surface temperature data set (HadISST version 1.1 [*Rayner et al.*, 2003]), and climatologies are based on the 1979–1999 period. Observed monthly mean values were interpolated to the model grid using bilinear interpolation over the open ocean and by averaging nearby grid values in coastal regions. Arctic sea ice area varies while thickness is specified to be 2.5 m. It is not expected that specifying ice thickness will significantly influence the results since the summer atmosphere in a regional climate model was shown to be insensitive to changes in sea ice thickness [*Rinke et al.*, 2006]. The conductive heat flux through sea ice is small during summer regardless of ice thickness because the ocean and near-surface air temperatures are similar. Global SSTs and sea ice in the Southern Hemisphere (specified to be 1 m) evolve according to the mean seasonal cycle in order to isolate the influence of Arctic sea ice. In regions where the ice extent was lower than the mean extent, the exposed ocean was set to the climatological SST; when the ice area expanded above normal, SSTs were blended from −1.8°C (the temperature at which there is 100% ice cover) at the ice edge with climatological values from two grid boxes (2.8° latitude × 2.8° longitude) seaward from the ice edge. This method was employed to smooth the temperature gradient between ice and ocean. In the extent experiments, the monthly Arctic sea ice values were specified to cover 100% of the grid square if the observed monthly averaged concentration exceeded 15%; otherwise, the grid square was set to be ice free. Monthly mean ice and SST values were linearly interpolated in time from mid monthly values to obtain smoothly varying daily extents and concentrations. As a result, the transition from no ice to complete ice cover in a grid square is not instantaneous in the extent simulations; instead, the amount of ice linearly evolves between 0% and 100% within the 30-day period when ice forms or melts. While this provides for a smooth transition of the ice edge in space and time, and is probably more realistic than an instantaneous transition, it also introduces fractional ice cover into the extent experiments.

2.2. Experiment Design

We focus this study on the summer of 1995, which contained minimum sea ice extent over the entire Arctic from June to September during recent years, with the exception of 2007 (Figure 1). Ice area during 2005 and 2006 was just slightly above that of 1995. Typically, Arctic summer sea ice extent reaches a minimum in mid September of approximately 5×10^6 km^2, though recent minima (e.g., 2005 through 2007) have been consistently lower. Three model experiments have been performed in which Arctic sea ice varies according to the following observations:

- Ice extent varies over April to October of 1995 (Sum95e).
- Ice concentration varies over April to October of 1995 (Sum95c).

The experiments are designated, in parentheses above, by the season, year, and ice configuration. We also performed an extended (55 years) control simulation in which ice extent repeats the same seasonal cycle each year based on the average of the 1979–1999 period (Cntle),

The Sum95e and Sum95c experiments consist of an ensemble of 51 CCM3 simulations that extend from April to October. Each member of the ensemble is initialized from a different 1 April from years 5–55 of the control extent experiment (Cntle). A discussion quantifying the relationship between signal-to-noise ratio and ensemble members

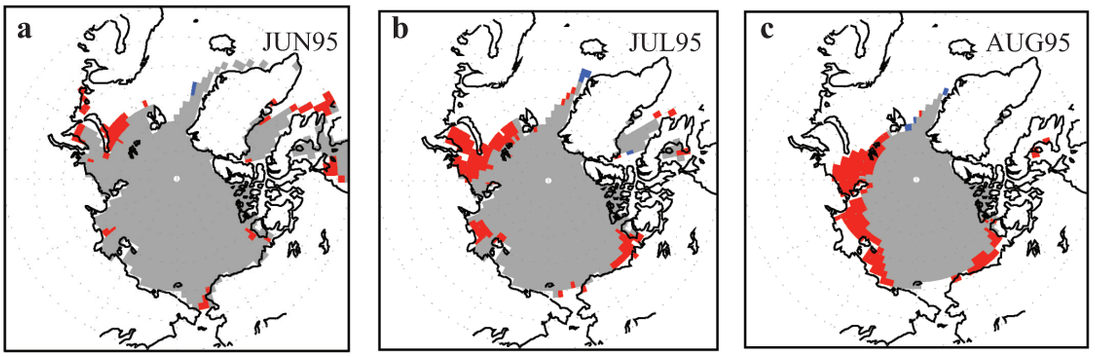

Plate 1. Evolution of sea ice extent during the boreal summer months of June–August of 1995. Blue (red) squares indicate enhanced (reduced) ice when compared to the monthly mean ice extent (represented by gray plus red areas).

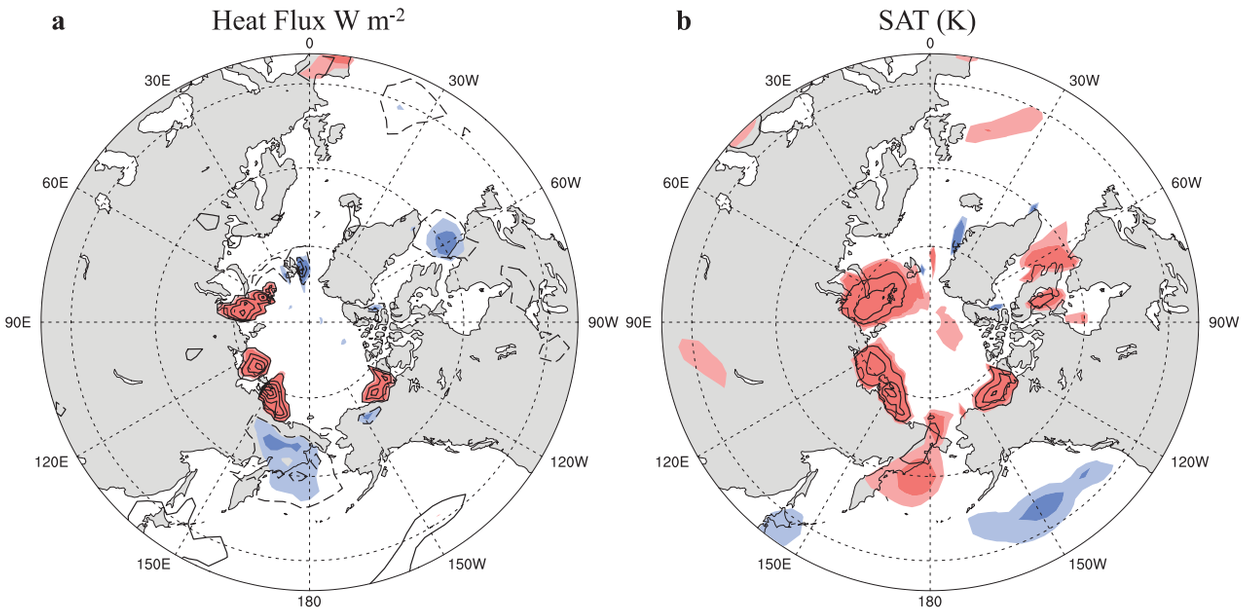

Plate 2. (a) Net surface heat flux anomalies (sensible plus latent plus longwave) felt by the atmosphere and (b) surface air temperature (SAT) anomalies in August of Sum95e. Dark (light) red or blue indicates statistical significance at the 99% (95%) or greater level based on a pooled variance *t* test. Confidence interval (CI) is 5 W m^{-2} and 0.5 K for heat flux and SAT, respectively. This is a polar stereographic view from 40° to 90°N.

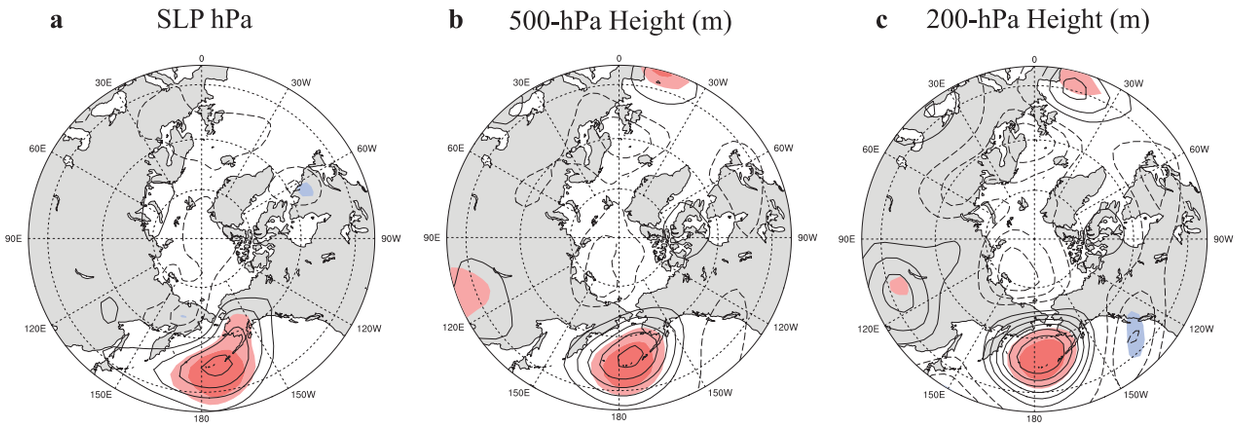

Plate 3. Sum95e (a) SLP anomaly response to reduced sea ice during August and geopotential height anomalies at (b) 500 hPa and (c) 200 hPa. Dark (light) shading indicates statistical significance at the 99% (95%) or greater level based on a pooled variance *t* test. The CI is 0.5 hPa for SLP and 5 m for geopotential height. This is a polar stereographic view from 40° to 90°N.

is given by *Alexander et al.* [2004]. The modeling results are generally presented as monthly anomalies constructed by averaging over the 51 ensembles and subtracting the corresponding long-term monthly mean over the last 51 years of the control simulation.

The discussion in this paper focuses on the model response during August of 1995. Ice anomalies evolve during the simulation based on observed April to October ice conditions. In 1995, ice was below normal in the Kara-Barents seas in July and throughout the Eurasian Arctic and in the Chukchi and Beaufort seas during August (Plate 1) and September. The atmospheric response in June and July was generally weak and will not be discussed. This may be a consequence of overall smaller sea ice anomalies during these months.

2.3. Atmospheric General Circulation Model

The CCM (version 3.6) is the atmospheric GCM used in this study; it has 18 vertical levels and a horizontal spectral resolution of T42, which is approximately 2.8° latitude by 2.8° longitude. *Kiehl et al.* [1998] describe the model physics, while *Hack et al.* [1998] and *Hurrell et al.* [1998] evaluate the model's climate with a global perspective while *Briegleb and Bromwich* [1998a, 1998b] evaluate the polar climate. Model evaluations relevant for this study will be briefly outlined.

Hurrell et al. [1998] find that while the subtropical summer time SLPs are higher than observed, CCM3 captures the key interseasonal shifts of the subtropical highs. The newer Community Atmosphere Model (CAM3) displays similar SLP features as CCM3 [*Hurrell et al.*, 2006]. SLP over the Arctic is higher than observed, and none of the Atmospheric Model Intercomparison Project models investigated by *Bitz et al.* [2002] capture the observed closed low over the central Arctic during summer. An investigation by *DeWeaver and Bitz* [2006] shows that JJA Arctic SLP in the Community Climate System Model, version 3 (CCSM3) is too high, a feature that is particularly prominent at T42 resolution. They find that in the model there is subsidence due to a thermally direct mean meridional circulation while reanalysis data indicate rising motion with an indirect Ferrel cell in the Arctic. Consistent with these studies, the Cntle simulation SLP is 5–7 hPa too high compared to the National Centers for Environmental Prediction/National Center for Atmospheric Research (NCAR) reanalysis over the Arctic during August (not shown).

Briegleb and Bromwich [1998b] find that CCM3 summer time tropospheric temperatures in the Arctic are cooler than observed by 2°–4°K, while precipitation minus evaporation (P − E) compares favorably with observations. The Arctic July total cloud amount in CCM3 is similar to observations [*Briegleb and Bromwich*, 1998a, Figure 10b], but the cloud water path is too high resulting in clouds that reflect (emit) excessively in the shortwave (longwave) range [also see *Gorodetskaya and Tremblay*, this volume].

While the model has some deficiencies over the Arctic, e.g., it is colder and wetter than observed (which also occurs in most other atmospheric general circulation models [*Randall et al.*, 1998]), many aspects of the Earth's climate are well simulated. This is a well-documented model that has been used in numerous studies of the impact of sea ice on the atmosphere [e.g., *Deser et al.*, 2004; *Magnusdottir et al.*, 2004; *Alexander et al.*, 2004].

2.4. Linear Baroclinic Model

To understand the mechanism for the large-scale response over the North Pacific to reduced Arctic sea ice in August, we forced a LBM with daily mean diabatic heating and transient eddy heat and vorticity fluxes, similar to *Deser et al.* [2007], from Cntle and Sum95e. The LBM [see *Peng et al.*, 2003] is based on the primitive equations configured with T21 horizontal resolution and 10 equally spaced pressure levels from 950 to 50 hPa. The model is linearized about the CCM3 basic state obtained from the long-term August mean in Cntle. The LBM includes dissipation in the form of Rayleigh friction in the momentum equation and Newtonian cooling in the thermodynamic equation, as well as biharmonic thermal diffusion. The Rayleigh and Newtonian damping time scales are 1 day at 950 hPa transitioning linearly to 7 days above 700 hPa. The LBM is integrated for 31 days.

The pattern of the CCM3 response to sea ice forcing is diagnosed by comparing the LBM responses to anomalous diabatic heating and transient eddy fluxes from Cntle and Sum95e. The transient eddies are based on 14-day high-pass-filtered data, constructed by subtracting the 11-day running means from the raw daily data (the half-power point of this filter is 14 days).

3. RESULTS AND DISCUSSION

3.1. Local Arctic Response

The model atmosphere displays a local thermal response to reduced western Arctic sea ice extent. The net heat flux anomalies resulting from the reduced sea ice are 10–25 W m^{-2} from the ocean to the atmosphere (Plate 2a). The sensible heat flux is the dominant form of heating contributing about 4–8 W m^{-2}, followed by latent heat flux at 2–6 W m^{-2} and then longwave at 2–4 W m^{-2}. Increased upward (downward) directed longwave radiation of 2 W m^{-2} is associated with a decrease (enhanced) in low-level clouds of 2%. It is not sur-

prising that daily model turbulent heat fluxes differ by an order of magnitude between summer and winter. Ignoring wind speed and drag coefficients, sensible heat flux is proportional to the temperature difference between the ocean and near-surface air, which is on the order of 1°K in summer and 10°K in winter. The winds are generally stronger in winter, which increases the fluxes, but the polar atmosphere is also relatively stable which damps turbulent fluxes. The sensible heat flux differences between winter and summer can be explained by the seasonal difference in vertical temperature gradients. Parallel arguments can be made for latent heat fluxes. Plots of model net surface solar flux, albedo, surface temperature, cloud cover, and specific humidity are described in the text but will not be shown. Anomalies of net surface solar heat flux are directed into the ocean and are on the order of 15–30 W m^{-2} where high-albedo ice is replaced by a lower-albedo ocean. However, the shortwave anomalies do not impact our simulation since the ocean temperature and ice are fixed and are not included in the net heat flux calculation. In nature, the enhanced solar flux into the surface would melt more ice or act to warm the ocean in the shallow ice-free seas. However, we specify the observed evolution of sea ice and argue that any ice melt from increased net solar radiation into the ocean is represented by the observed sea ice conditions.

The surface temperature anomalies associated with the reduced ice area are between 0.5° and 1.5°C where climatological ocean sea surface temperatures replace sea ice. The surface air temperature (Plate 2b) warms throughout the Arctic with strongest warming present over the Kara-Barents and East Siberian seas and over eastern Siberia with anomalies between 0.5° and 1.5°C. This low-level warming is associated with small decreases in sea level pressure and geopotential heights that are not statistically significant (Plate 3). The air temperature warming is relatively shallow over the Arctic with no significant anomalies at or above 925 hPa. There is a significant increase in convective precipitation (1 mm d^{-1}), convective clouds (1–2%), and middle-level clouds (2–4%) in the Laptev Sea where sea ice is reduced. In the Kara Sea over the reduced ice extent, there is a significant decrease in total cloud cover (2–4%), which results from less low, medium, and high clouds. There are no significant changes in large-scale precipitation over the Arctic. The CCM3 positive SLP bias in the control simulation discussed earlier could play a role in the small convective response over the Arctic.

3.2. Midlatitude Response

The model response to reduced western Arctic sea ice in the North Pacific is characterized by changes in the large-scale circulation and displays significant anomalies in eastern Siberia (65°N, 165°E) and over the ocean storm track region (55°–60°N). In far eastern Siberia, negative sensible and longwave heat flux anomalies total 5 W m^{-2} (Plate 2a) while downward solar heat flux is reduced by 5 W m^{-2}, resulting in a net heat flux change of near zero. Surface temperature and surface air temperatures are warmer by up to 1.0°C and 0.5°C (Plate 2b), respectively. Increased convective and large-scale precipitation is collocated with increases in specific humidity (up to 2 g kg^{-1}). Total cloudiness in eastern Siberia increases by up to 4% with more clouds at all levels. The SLP and geopotential height anomalies are weakly negative and not significant over eastern Siberia. Since the net surface heat flux anomalies are weak, the warmer moister atmosphere results from southerly advection associated with the circulation changes over the North Pacific.

The SLP response is characterized by a significant anomalous high over the North Pacific with a central maximum of 2 hPa (Plate 3a). At 500 and 200 hPa the anomalous high in the North Pacific reaches 20 and 30 m (Plates 3b and 3c), respectively, displaying an equivalent barotropic structure. This pattern is characteristic of the equilibrium response to a midlatitude heating source attributed to transient eddy feedbacks that results from the interaction of the forced anomalous flow and the storm tracks [*Kushnir and Lau*, 1992; *Ting and Peng*, 1995; *Peng and Whittaker*, 1999]. The response to reduced sea ice does not project on the dominant modes of model variability, and this is discussed further in section 4. Additionally, these SLP and 500-hPa patterns compare favorably with observed circulation anomalies associated with reduced Eurasian sea ice, and this is briefly addressed at the end of section 4.

The model displays a response in the North Pacific storm track region with significant total precipitation anomalies (Plate 4). Anomalies of large-scale precipitation are about twice as large as those of convective precipitation (not shown). The magnitude of the total precipitation response reaches values of 25% of the mean climatological precipitation (Plate 4, contours). The mean and anomalous precipitation patterns suggest a weakening of the main North Pacific storm track and a slight enhancement on the poleward side. In other words, the storm track shifted northward and weakened, which is consistent with a weakened meridional temperature gradient [see *Hartmann*, 1994, section 9.5]. The mechanisms associated with the strengthening of the subtropical high and the storm track changes are not well understood, and a further discussion is included in section 4. Note that the precipitation maximum on the south coast of Alaska is associated with orography, and the reduced onshore winds associated with the SLP response is likely responsible for the coastal precipitation anomalies.

Storm track variability as indicated by 2- to 8-day bandpass-filtered variance statistics for 500-hPa height variance,

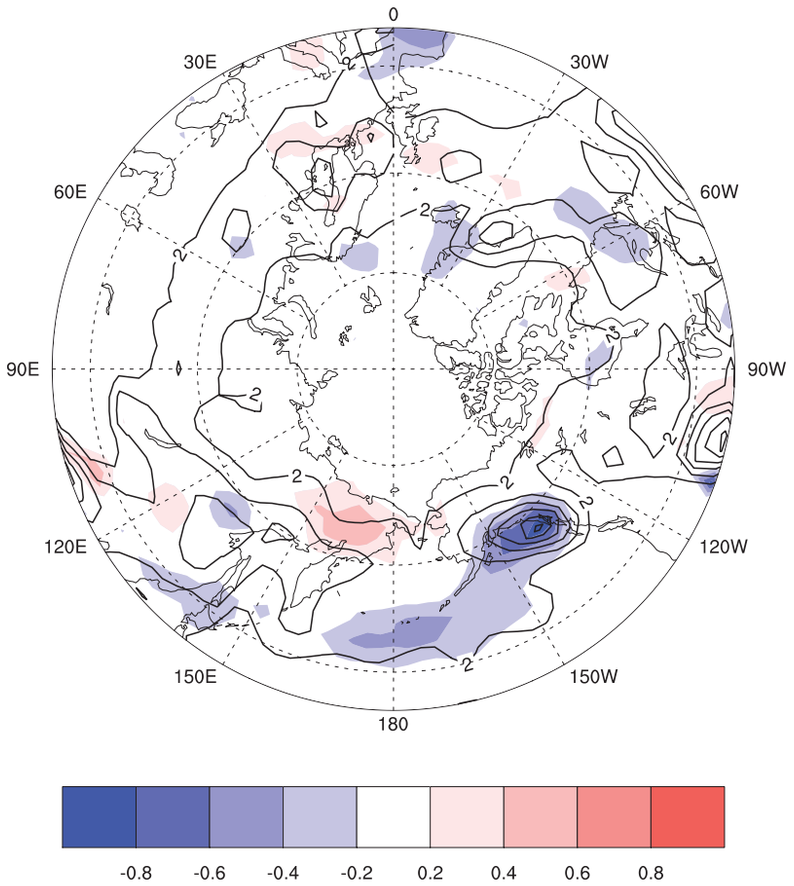

Plate 4. Sum95e total precipitation anomalies (shaded) are overlaid with contours of mean total precipitation from the control simulation (Cntle) during August. Anomaly magnitudes greater than 0.2 mm d^{-1} are statistically significant at the 95% or greater level based on a pooled variance *t* test. CI is 0.2 mm d^{-1} for total precipitation anomalies, where red (blue) shading represents positive (negative) anomalies and values between −0.2 and +0.2 are white. CIs for mean precipitation are 2, 3, 4, 5, 6, and 7 mm d^{-1}.

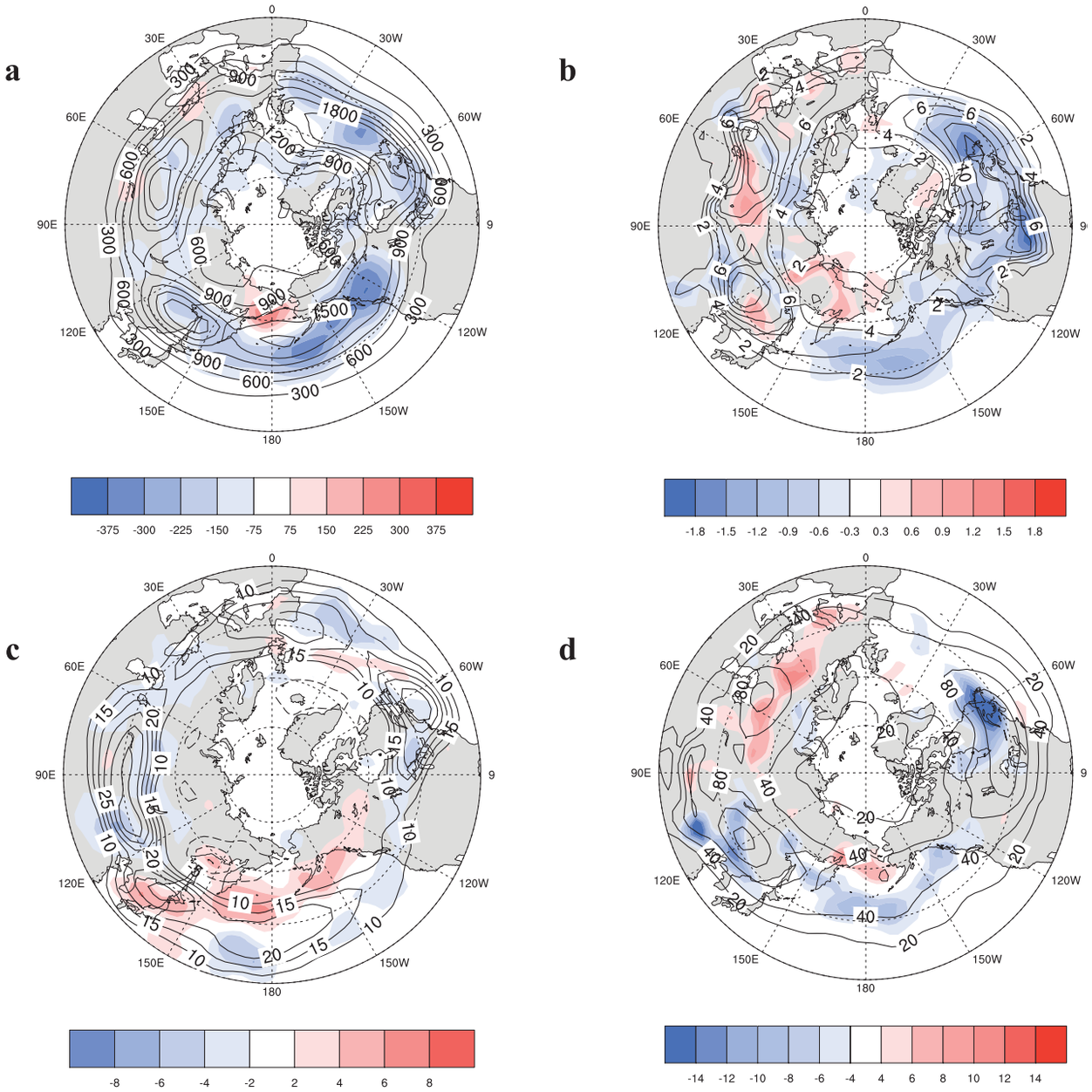

Plate 5. August storm track variability as indicated by 2- to 8-day band-passed (a) 500-hPa geopotential height variance, (b) 850-hPa v'T', (c) 200-hPa u'v', and (d) 500-hPa omega variance. The Cntle mean for each quantity is shown by contours, and the Sum95e-Cntle anomalies are shown by shaded values. The units are m^2, m s^{-1} C, m^2 s^{-2}, and 10^{-4} Pa^2 s^{-2} for Plates 5a, 5b, 5c, and 5d, respectively. In the Pacific sector, statistically significant anomalies have approximate magnitudes greater than 225 m^2, 0.9 m s^{-1} C, 5 m^2 s^{-2}, and 6 $(10)^4$ Pa^2 s^{-2} for Plates 5a, 5b, 5c, and 5d, respectively.

850-hPa transient heat flux, 200-hPa transient momentum flux, and 500-hPa omega variance are shown in Plate 5. All of the mean model storm track measures in the control simulation (Cntle) display maxima in the eastern Pacific, eastern North Atlantic, and central Eurasia (Plate 5, contours). These maxima are qualitatively similar to observed maxima [see *Zhang et al.*, 2004, Figure 2b]. Decreased ice (Sum95e) leads to a general weakening of the storm tracks throughout the hemisphere (Plate 5, blue shading); however, the primary significant response is in the Pacific sector. There is a small region of enhanced storm track activity over the east Siberia–Bering Sea region (Plate 5, red shading). Note that an increase in 500-hPa height variance signifies both the passage of more highs as well as lows. The band-passed 500-hPa omega vertical velocity variance anomalies (Plate 5d) are consistent with the height variances. The 2- to 8-day band-passed 850-hPa v'T' or transient eddy heat fluxes are reduced over the mean storm track in the North Pacific and enhanced to the north in eastern Siberia–Bering Sea. In addition, the transient eddy heat fluxes at 850 hPa display significant reductions in storm track activity over North America into the North Atlantic. The 2- to 8-day band-passed 200-hPa u'v' transient eddy momentum fluxes are characterized by increased (decreased) poleward momentum flux to the north (south) of the mean storm track in the North Pacific, which is consistent with the anomalous high in geopotential height response (Plate 5c). Referring to the geopotential tendency equation, the convergence of vorticity (or momentum) fluxes north of the mean storm track is consistent with the positive equivalent barotropic height anomalies [*Lau and Nath*, 1991]. The significant precipitation anomalies (Plate 4) are consistent with the weakening and northward displacement of the North Pacific storm track (Plate 5).

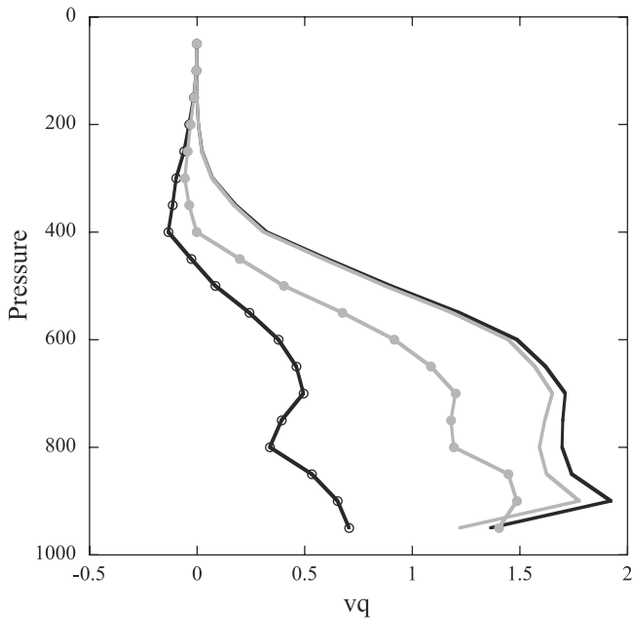

Figure 2. August meridional moisture transport in units of g kg^{-1} m s^{-1}. Vertical profiles are shown at 70°N for Cntle (black lines) and Sum95e (grey). Zonal averages over all longitudes (0°–360°) are shown by the lines with no circles. Averages over the Pacific sector (160°–200°E) are displayed by the lines with circles.

3.3. Diagnosis of Forcing

One possible mechanism for the remote response over the North Pacific involves a Rossby wave train (albeit weak in this case) that is initially excited by diabatic heating anomalies in the Arctic. This wave train propagates into the North Pacific, where through interactions with the storm tracks, an anomalous high is generated over the center of the basin. This mechanism resembles the large-scale eddy feedback described by *Peng et al.* [2003] with the exception that the boundary forcing was close to the storm track in their study.

Diabatic heating anomalies are constructed to investigate the forcing of the atmosphere by reduced sea ice extent. The Cntle mean vertically integrated diabatic heating is shown by contours in Plate 6a and displays cooling of 50–100 W m^{-2} over the Arctic. The vertically integrated diabatic heating displays positive anomalies where Arctic sea ice is reduced of 15–25 W m^{-2}, which is about 10–20% of mean. There is a decrease in the region of the North Pacific storm track (Plate 6a) A vertical cross section through the largest diabatic heating anomalies indicates that in the Arctic the positive heating anomalies are located below 800 hPa, and the negative anomalies in the North Pacific penetrate up to 400 hPa (Plate 6b).

The linear baroclinic model described in section 2 was forced with the transient eddy vorticity fluxes, transient eddy heat fluxes, and mean diabatic heating separately to diagnose the key forcing behind the atmospheric response patterns. The LBM response (Plates 7c–7h) is compared to the full GCM anomalies (Plates 7a and 7b) at 500 and 950 hPa. This diagnostic model analysis reveals that the transient eddy vorticity fluxes are responsible for maintaining the anomalous high in the North Pacific, whereas transient eddy heat fluxes and diabatic heating yield a negligible response. The LBM response to the total transient eddy and diabatic heating is nearly indistinguishable from the response to the transient eddy vorticity fluxes. The primary role of transient eddy vorticity fluxes has been noted in previous studies [*Peng and Whitaker*, 1999; *Deser et al.*, 2007]. The LBM analysis does not reveal how the reduced Arctic ice anomalies induced the eddy momentum fluxes over the North Pacific, perhaps in-

dicating that the diabatic heating anomalies over the Arctic are too shallow and weak to drive the large-scale response. In other words, we argue for an indirect mechanism via the storm track for the ice anomalies to impact the North Pacific rather than impacting the flow directly.

3.4. Partial Ice Reduction Sensitivity Experiments

To investigate the sensitivity of the atmospheric response to the placement of the ice anomalies, three experiments were conducted where CCM3 was forced with partial sea ice anomalies from Sum95e ice conditions. The ice was removed in the Kara (Sum95ke) (Plate 8a), Laptev–East Siberian (Sum95le) (Plate 8b), and Beaufort (Sum95be) (Plate 8c) seas. The integration and processing procedure for the partial ice experiments was similar to one used for the full anomaly case (Sum95e) to construct a 51 ensemble member response. The largest positive net surface heat flux anomalies (not shown) into the atmosphere are located directly over grid boxes where ice was removed and are identical to the analogous anomalies from the Sum95e (Plate 2a) simulation. Sum95ke and Sum95le display weak negative heat flux anomalies over eastern Siberia, and Sum95be has significant negative anomalies around 5 W m^{-2}.

Surface temperature and SAT responses to the partial ice anomalies are characterized by warming in the vicinity of the reduced ice anomaly, and the magnitudes are nearly identical to those from the full ice experiment. Warm SAT anomalies in far eastern Siberia–Bering region are significant in Sum95le and Sum95be, with the Beaufort ice forcing the largest response in eastern Siberia. The eastern Siberia positive SAT anomalies are consistent with positive advection associated with the anomalous low (high) over the Siberia (North Pacific).

The atmospheric SLP and geopotential height responses to the partial ice experiments resemble that of Sum95e. A weak high over the Kara Sea, a weak low over east Siberia stretching into the Chukchi Sea, and the anomalous high in the North Pacific are all common features of the SLP and geopotential height response patterns to partial ice anomalies (Plates 8d–8i). The individual responses shown in Plate 8 are weaker than the response in Sum95e; however, the sum of these three partial ice experiment response patterns in Plate 8 for SLP and 500-hPa geopotential height is nearly twice as strong as the response to the total ice anomaly (Sum95e). Ice reductions in the Laptev–East Siberian and Beaufort seas produce a statistically significant response in the North Pacific. The anomalous low (SLP and 500-hPa height) over east Siberia is stronger in the Beaufort partial ice experiment than in Sum95e. This suggests that the model atmosphere is sensitive to ice reductions in all three of these regions and the induced climate anomalies are fairly similar.

The precipitation response (not shown) patterns to the partial ice anomalies are sensitive to the location of the ice anomalies. The positive precipitation anomalies over eastern Siberia are weakly evident in Sum95le and are significant in Sum95be. The negative precipitation anomalies in the mean model storm track zone are overall largest for Sum95be, largest over south coastal Alaska for Sum95ke, and significant for a limited area over the ocean for Sum95le. The sum of the precipitation anomalies for the three partial ice experiments is slightly larger than the precipitation anomalies for Sum95e.

3.5. Ice Concentration Experiments

The August 1995 experiment was repeated using ice concentration anomalies (Sum95c) (Plate 9a). The net surface heat fluxes (not shown) and SAT were similar to Sum95e. One feature different from the Sum95e ensemble average is an area of significant negative surface air temperature anomaly between 120° and 150°E in eastern Siberia (Plate 9b). The Sum95c SLP response has a weaker anomalous high in the North Pacific and a stronger anomalous low in eastern Siberia compared to the extent experiment. The atmospheric response at 500 hPa is similar though it looks more like a wave train in the Pacific (Plate 9c). During summer the contrast between using ice extent and concentration is small, whereas the differences are larger in winter [*Alexander et al.*, 2004]. The area of open water is slightly larger during summer than winter (compare the difference between the two time series in Figure 1 in 1995 with the difference for 1996 in Figure 1 of *Alexander et al.* [2004]), but the larger air-sea temperature contrast in winter strongly influences the turbulent heat fluxes. Anomalies for Sum95c are constructed by taking the difference between the concentration experiment (Sum95c) and an extent control (Cntle). Large ice anomaly differences exist between the concentration control (Cntlc) and Cntle, complicating the interpretation of the differences when a concentration control is used, and thus the Cntlc experiments are not used as a baseline here.

4. CONCLUSIONS

This study employs an atmospheric global climate model (CCM 3.6) to examine the atmospheric response to observed variations in sea ice during the summer of 1995, which had the lowest ice extent during June–September in the Arctic over the last ~30 years with the exception of 2007. (The September ice minimum has been near or well below the 1995 levels since 2002 [*Stroeve et al.*, 2008]). Sea ice was

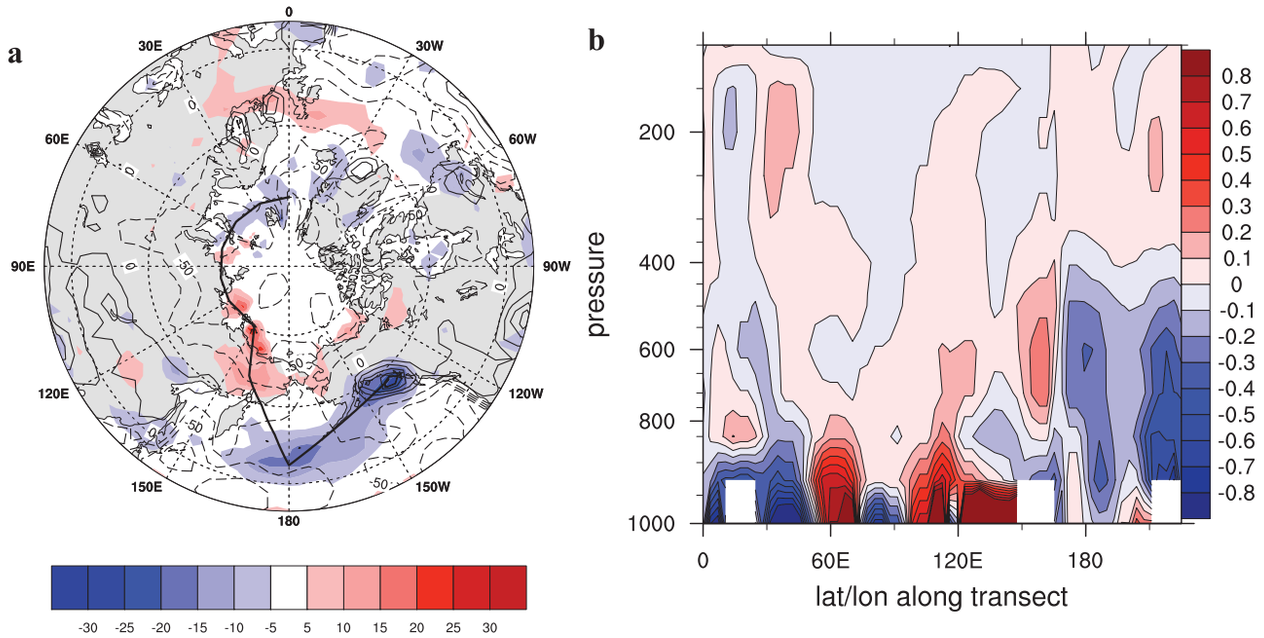

Plate 6. August (a) mean (Cntle, contours) and anomalous (Sum95e-Cntle, shaded) vertically integrated diabatic heating rate. The path of the transect is shown by a thick black line in Plate 6a. (b) Transect through the Arctic into the North Pacific showing total diabatic heating rate anomalies. The units are W m^{-2} in Plate 6a for both shaded and contoured fields. CI is 0.1 K d^{-1} in Plate 6b. The total diabatic heating rate is the sum of convective adjustment, solar heating, longwave heating, vertical diffusion, and horizontal diffusion.

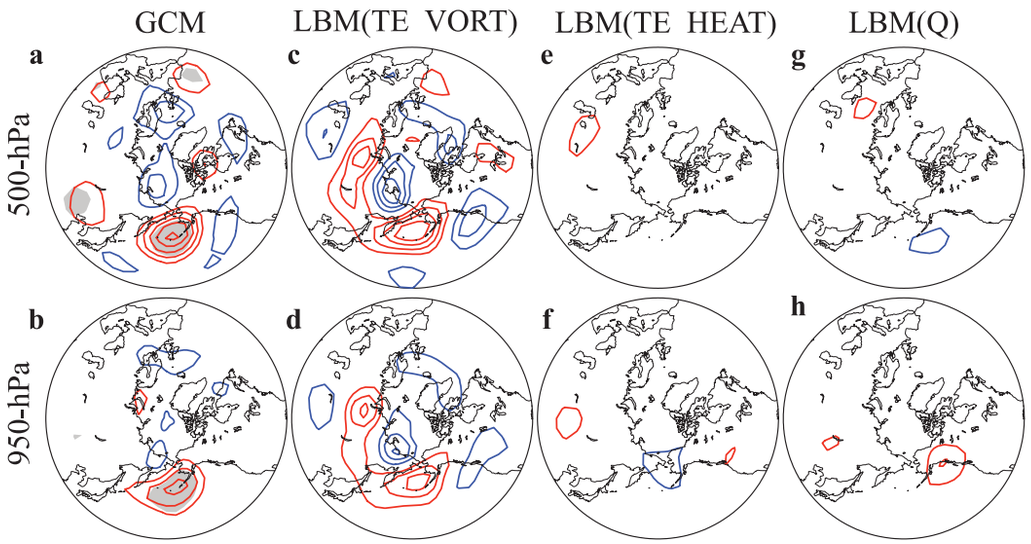

Plate 7. LBM results in August for Sum95e. Geopotential height GCM response to reduced sea ice at (a) 500 hPa and (b) 950 hPa. Individual LBM response to (c and d) transient eddy vorticity, (e and f) transient eddy heat fluxes, and (g and h) diabatic heating. CI is 5 m where red (blue) signifies positive (negative) height anomalies. The LBM response has been multiplied by 2.5 to match the magnitude of the GCM response.

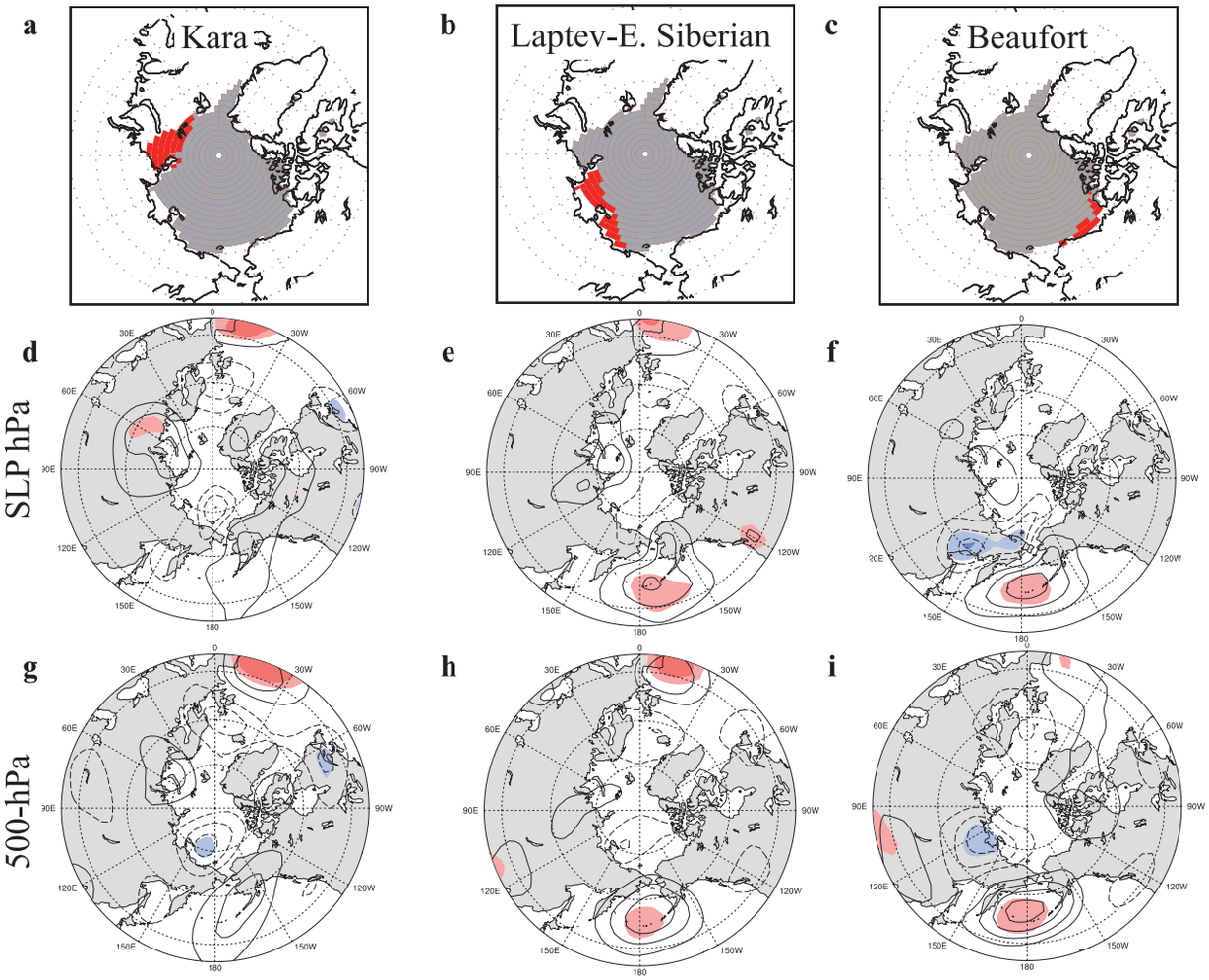

Plate 8. August sea ice anomalies for (a) Sum95ke, (b) Sum95le, and (c) Sum95be where ice is reduced only in the Kara Sea, Laptev–East Siberian seas, and the Beaufort Sea, respectively. (d–f) SLP anomalies and (g–i) 500-hPa geopotential height anomalies in response to reduced sea ice in individual seas. Dark (light) shading indicates statistical significance at the 99% (95%) or greater level based on a pooled variance *t* test. CI is 0.5 hPa for SLP and 5 m for geopotential height.

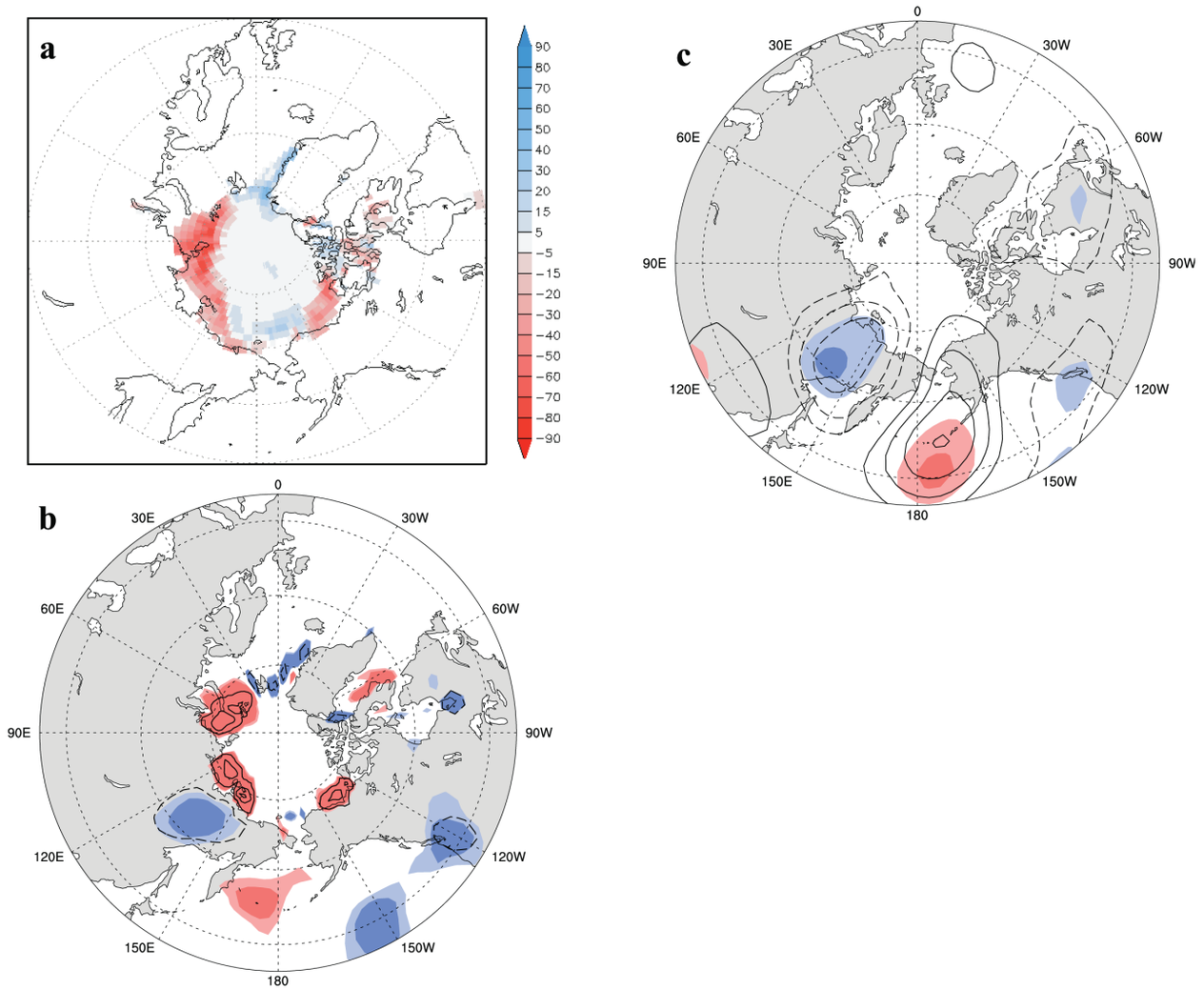

Plate 9. Sum95c August ice concentration anomalies in (a) percent of area, (b) surface air temperature with a CI of 0.5 K, and (c) 500-hPa height with a CI of 5 m.

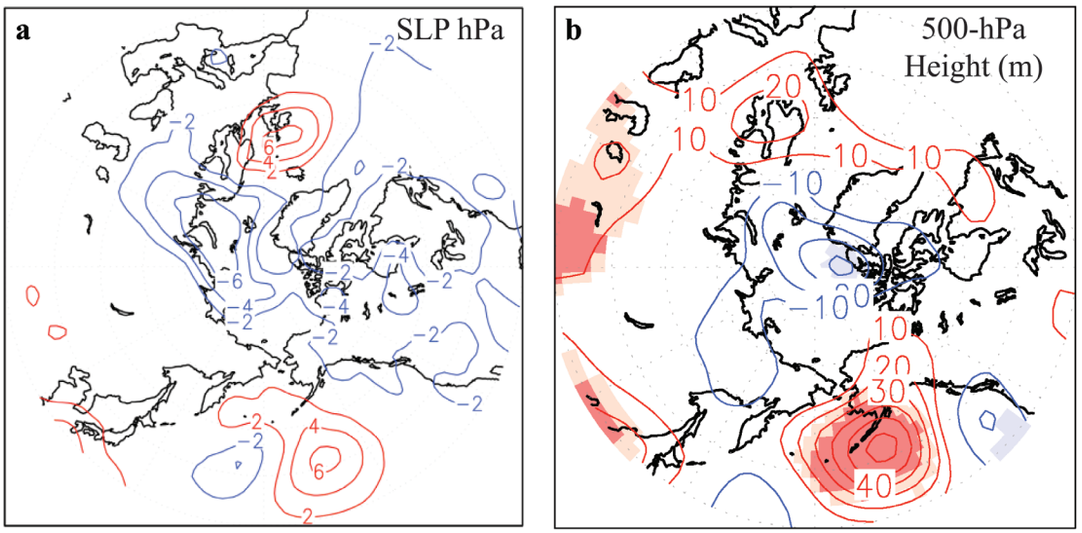

Plate 10. (a) Observed SLP anomalies in August 1995 in hPa. The mean climatology is based on the years 1968–1996, and the CI is 2 hPa. (b) Observed 500-hPa geopotential height composites based on reduced ice in the Kara Sea region. The 500-hPa height is in meters. Shading indicates statistical significance at the 95% or greater level based on a pooled variance *t* statistic. The years used in this composite are 1979, 1984, 1985, 1994, 1995, 1997, and 2000.

prescribed as ice extent (ocean grid box is either completely covered or totally ice free) or ice concentration (partial grid box covered in ice allowed) based on monthly observations. Fifty-one ensemble members were integrated from April to October 1995 using climatological sea surface temperatures. The control simulation was integrated with global climatological sea ice extent and SSTs. The strongest response was found during the month of August when the ice area is nearing its minimum for the year.

The Arctic displays a local thermal response with increased surface heat fluxes (sensible plus latent plus longwave) into the atmosphere, warmer SATs, and a weak decrease in SLP. The atmospheric response is also characterized by an anomalous high in sea level pressure in the North Pacific, which is part of a northward expansion of the summertime subtropical high. The atmospheric response with height is equivalent barotropic, and the anomalous high increases in amplitude with height and is significant at 200 hPa. There is a significant decrease (increase) of precipitation along the eastern (northwestern) part of the mean North Pacific storm track, consistent with the 500-hPa geopotential height variances and 850-hPa transient eddy heat fluxes that indicate enhanced storminess north of the mean storm track and a decrease over the mean storm track in the North Pacific.

Additional climate experiments were conducted to determine the model sensitivity to the location of sea ice anomalies. When ice reduction is limited to only the Kara Sea, the Laptev–East Siberian seas, or the Beaufort Sea the atmospheric response patterns for SLP, geopotential height, and precipitation are similar but weaker than when the sea ice is reduced for all the seas, suggesting that the model is sensitive to sea ice anomalies in all three regions. The area of the significant response increases from the Kara to the Beaufort, which is closest to the North Pacific. These results are analogous to a GCM study by *Geisler et al.* [1985] where the model Pacific North American response pattern (magnitude) is insensitive (sensitive) to the longitude of the tropical Pacific SST anomaly. The August 1995 experiment was repeated using ice concentration anomalies. The atmospheric response is similar though it resembles a wave train in the Pacific, similar to what *Alexander et al.* [2004] found for the response during winter to sea ice concentration extremes during winter of 1995–1996.

There has been increased interest recently in understanding mechanisms that force and maintain the summertime subtropical highs. In a zonal average, the subtropical highs are strongest in winter when subsidence associated with the Hadley circulation is most vigorous [*Grotjahn and Osman*, 2007]. However, the North Pacific (NP) high is strongest during boreal summer [see *Grotjahn*, 2004, Figure 1] and forms to the west of a region with strong thermal contrast between the cool ocean water and the warm North American landmass. *Miyasaka and Nakamura* [2005] employed a nonlinear spectral primitive equation model driven by zonally asymmetric diabatic heating and demonstrated that the strong surface thermal contrast can explain ~70% of the strength of the subtropical high, consistent with ideas first proposed by *Hoskins* [1996]. *Grotjahn* [2004] proposed that extratropical storms could provide forcing through transient eddies to maintain the subtropical high. *Grotjahn and Osman* [2007, Figure 2] present a conceptual picture of how ageostrophic motions arising from developing storms converge at the jet level, leading to sinking motion on the east side of the subtropical high and low-level divergence and southward motion that strengthens the subtropical high. They demonstrate that the variability of the NP high is dominated by midlatitude forcing during summer. Some of the features found in a warm season SLP composite analysis of observations by *Grotjahn and Osman* [2007] are qualitatively similar to circulation anomalies forced by reduced sea ice in CCM3. They find that SLP is weaker in parts of the Arctic Ocean when the North Pacific high is stronger and a stronger North Pacific high is associated with positive SLP anomalies on the northern flank of the high.

The LBM analysis suggests that the far field response is not forced directly by the Arctic ice but could rather be a consequence of the local Arctic response, which acts to reduce the flow between the Arctic and the lower latitudes. There may be some parallel with modeling studies of the response to Antarctic sea ice extremes. *Hudson and Hewitson* [2001] have examined the response to realistic monthly varying sea ice and SST anomalies in the Antarctic. They found that where the sea ice has been reduced and ocean exposed, the SAT increases and there is a strengthening and a southward extension of the subtropical high-pressure belt. *Raphael* [2003] found complementary results using the NCAR CCSM.

The dominant mode of variability determined from Cntle empirical orthogonal function (EOF1) of SLP in August resembles the Arctic Oscillation. The model response to reduced summer ice does not correspond to the dominant mode for SLP or 500-hPa heights. Given results from previous studies we hypothesize that the reason that this occurs is because the ice anomaly is located far from the storm tracks. *Honda et al.* [1999] and *Alexander et al.* [2004] found that wintertime North Pacific ice edge anomalies, located well north of the average storm track, do not project on the dominant modes of the GCM. In contrast, *Deser et al*. [2004], *Magnusdottir et al.* [2004], and *Alexander et al.* [2004] found that the GCM response to ice edge anomalies in the North Atlantic during winter strongly project on the dominant modes of variability. The storm track is located nearly

above the ice edge. *Glowienka-Hense and Hense* [1992] forced a GCM with a polynya in the Kara Sea. Their ice anomaly was in the pack ice far from the ice edge and their response was weak local heating with a general weakening of the Atlantic storm track, very similar to our Sum95e response. They argue that open water in the ice pack yields a different response than at the ice edge.

Perhaps, a parallel can be drawn from the better understood topic of the atmospheric response to midlatitude SSTs, where it has been shown that the atmospheric response is highly sensitive to the location of the SST forcing with respect to the climatological flow [see *Kushnir et al.*, 2002, and references therein]. A conundrum in our results is that the partial ice anomaly experiments (Sum95ke, Sum95le, and Sum95be) all yield very similar patterns to each other and the full ice anomaly. This finding would be consistent with the response projecting on a key mode of natural variability. So, having examined the first four EOF patterns, it is unclear at this point whether a less dominant mode of variability is being excited by the sea ice anomalies.

The atmospheric circulation response to extreme sea ice anomalies is explored in the context of how they may feed back onto the sea ice. A strong negative feedback was suggested in the winter sea ice forcing GCM studies [*Alexander et al.*, 2004; *Deser et al.*, 2004] where the atmospheric response was of the opposite sign to the circulation that initially forced the sea ice anomalies. The exchanges of latent heat between the Arctic north of 70°N and the midlatitudes are largest during August as shown in a study of the observed energy budget of the Arctic [see *Serreze et al.*, 2007, Figure 6]. Increased moisture in the Arctic has been shown to enhance downward longwave fluxes and possibly impact the sea ice [*Francis and Hunter*, 2006]. Figure 2 presents the ensemble averaged vertical profiles of meridional moisture transport in Sum95e (grey line) and Cntle (dark line) at 70°N averaged over all longitudes (plain lines) and in the Pacific sector (lines with dots) for 160°–200°E. The global average moisture transports into the Arctic cap do not differ much between Cntle and Sum95e. However, in the Pacific sector the poleward moisture transport is enhanced notably in the lower 500 hPa. This increase of moisture would trap more longwave radiation and would work to delay ice formation, suggesting a positive feedback.

Observed atmospheric circulations present during reduced Arctic sea ice summers resemble the model response found in our study. During August 1995 the observed SLP field displays a negative anomaly over the Arctic and an anomalous high over the North Pacific (Plate 10a), which compares favorably with the model response to reduced sea ice. Plate 10b presents a 7-year composite of August 500-hPa anomalies based on summers with anomalously low sea ice in the Kara Sea. The anomalous high in the North Pacific is strikingly similar to the model response at 500 hPa (Plate 3b). This pair of panels was chosen to illustrate that the model response compares well with observations during 1995 as well as in a more robust measure based on composites. The similarity between the observations and the model results suggests that realistic Arctic sea ice decreases may force circulation changes in the North Pacific and warrants further examination.

Acknowledgments. This work benefited from discussions with H. Nakamura, W. Robinson, S. Peng, R. Grotjahn, N. Mölders, and I. Polyakov. S. Bourne is thanked for a careful reading of the manuscript. We deeply appreciate the through critiques received from an anonymous reviewer and E. DeWeaver that improved this paper. This research was supported by a grant from the NOAA's Arctic Research Office issued through the International Arctic Research Center (IARC), the Frontier Research System for Global change through IARC, and by the Geophysical Institute. Support was also provided by the National Science Foundation through grant ARC-0327664. We also thank Steve Worley at NCAR for providing the HadISST data set for N. Raynor of the Hadley Centre. This work was supported in part by a grant of HPC resources from the Arctic Region Supercomputing Center at the University of Alaska Fairbanks as part of the Department of Defense High Performance Computing Modernization Program. We thank G. Robinson, C. Swingley, and W. Chapman for their assistance with various computer issues. Plots have been prepared using the open source software packages NCL (www.ncl.ucar.edu) and GrADS (www.iges.org/grads/).

REFERENCES

Alexander, M. A., U. S. Bhatt, J. Walsh, M. Timlin, and J. Miller (2004), The atmospheric response to realistic Arctic sea ice anomalies in an AGCM during winter, *J. Clim.*, *17*, 890–905.

Bitz, C. M., J. C. Fyfe, and G. M. Flato (2002), Sea ice response to wind forcing from AMIP models, *J. Clim.*, *15*, 522–536.

Briegleb, B. P., and D. H. Bromwich (1998a), Polar radiation budgets of the NCAR CCM3, *J. Clim.*, *11*, 1246–1269.

Briegleb, B. P., and D. H. Bromwich (1998b), Polar climate simulation of the NCAR CCM3, *J. Clim.*, *11*, 1270–1286.

Comiso, J. C., C. L. Parkinson, R. Gersten, and L. Stock (2008), Accelerated decline in the Arctic sea ice cover, *Geophys. Res. Lett., 35*, L01703, doi:10.1029/2007GL031972.

Deser, C., and H. Teng (2008), Recent trends in Arctic sea ice and the evolving role of atmospheric circulation forcing, 1979–2007, this volume.

Deser, C., J. E. Walsh, and M. Timlin (2000), Arctic sea ice variability in the context of recent atmospheric circulation trends, *J. Clim.*, *13*, 617–633.

Deser, C., G. Magnusdottir, R. Saravanan, and A. Phillips (2004), The effects of North Atlantic SST and sea ice anomalies on the

winter circulation in CCM3. Part II: Direct and indirect components of the response, *J. Clim.*, *17*, 877–889.

Deser, C., R. A. Thomas, and S. Peng (2007), The transient atmospheric circulation response to North Atlantic SST and sea ice anomalies, *J. Clim.*, *20*, 4751–4767.

DeWeaver, E., and C. M. Bitz (2006), Atmospheric circulation and its effect on Arctic sea ice in CCSM3 simulations at medium and high resolution, *J. Clim.*, *19*, 2415–2436.

Francis, J. A., and E. Hunter (2006), New insight into the disappearing Arctic sea ice, *Eos Trans. AGU*, *87*(46), 509.

Geisler, J. E., M. L. Blackmon, G. T. Bates, and S. Muñoz (1985), Sensitivity of January climate response to the magnitude and position of equatorial Pacific sea surface temperature anomalies, *J. Atmos. Sci., 42*, 1037–1049.

Glowienka-Hense, R., and A. Hense (1992), The effect of an Arctic polynya on the Northern Hemisphere mean circulation and eddy regime: A numerical experiment, *Clim. Dyn.*, *7*(3), 155–163.

Gorodetskaya, I. V., and L.-B. Tremblay (2008), Arctic cloud properties and radiative forcing from observations and their role in sea ice decline predicted by the NCAR CCSM3 model during the 21st century, this volume.

Grotjahn, R. (2004), Remote weather associated with South Pacific subtropical sea-level high properties, *Int. J. Climatol.*, *24*, 823–839.

Grotjahn, R., and M. Osman (2007), Remote weather associated with North Pacific subtropical sea-level high properties, *Int. J. Climatol.*, *27*, 587–602.

Hack, J. J., J. T. Kiehl, and J. W. Hurrell (1998), The hydrologic and thermodynamic characteristics of the NCAR CCM3, *J. Clim., 11*, 1151–1178.

Hartmann, D. (1994), *Global Physical Climatology*, 411 pp., Academic, London.

Honda, M., K. Yamazaki, H. Nakamura, and K. Takeuchi (1999), Dynamic and thermodynamic characteristics of atmospheric response to anomalous sea-ice extent in the Sea of Okhotsk, *J. Clim.*, *12*, 3347–3358.

Hoskins, B. (1996), On the existence and strength of the summer subtropical anticyclones, *Bull. Am. Meteorol. Soc.*, *77*, 1287–1292.

Hudson, D. A., and B. C. Hewitson (2001), The atmospheric response to a reduction in summer Antarctic sea-ice extent, *Clim. Res.*, *16*, 79–99.

Hurrell, J. W., J. J. Hack, B. A. Boville, D. L. Williamson, and J. T. Kiehl (1998), The dynamical simulation of the NCAR Community Climate Model version 3, *J. Clim., 11*, 1207–1236.

Hurrell, J. W., J. J. Hack, A. S. Phillips, J. Caron, and J. Yin (2006), The dynamical simulation of the Community Atmosphere Model version 3 (CAM3), *J. Clim.*, *19*, 2162–2183.

Kiehl, J. T., J. J. Hack, G. B. Bonan, B. A. Boville, and P. J. Rasch (1998), The National Center for Atmospheric Research Community Climate Model: CCM3, *J. Clim., 11*, 1131–1149.

Kushnir, Y., and N.-C. Lau (1992), The general circulation model response to a North Pacific SST anomaly: Dependence on time scale and pattern polarity, *J. Clim.*, *5*, 271–283.

Kushnir, Y., W. A. Robinson, I. Bladé, N. M. J. Hall, S. Peng, and R. Sutton (2002), Atmospheric GCM response to extratropical SST anomalies: Synthesis and evaluation, *J. Clim.*, *15*, 2233–2256.

Lau, N.-C., and M.-J. Nath (1991), Variability of the baroclinic and barotropic transient eddy forcing associated with monthly changes in the midlatitude storm tracks, *J. Atmos. Sci., 48*, 2589–2613.

Magnusdottir, G., C. Deser, and R. Saravanan (2004), The effects of North Atlantic SST and sea ice anomalies on the winter circulation in CCM3. Part I: Main features and storm track characteristics of the response, *J. Clim.*, *17*, 857–876.

Maslanik, J., S. Drobot, C. Fowler, W. Emery, and R. Barry (2007), On the Arctic climate paradox and the continuing role of atmospheric circulation in affecting sea ice conditions, *Geophys. Res. Lett.*, *34*, L03711, doi:10.1029/2006GL028269.

Maslanik, J. A., M. C. Serreze, and R. G. Barry (1996), Recent decreases in Arctic summer ice cover and linkages to atmospheric circulation anomalies, *Geophys. Res. Lett., 23*, 1677–1680.

Miyasaka, T., and H. Nakamura (2005), Structure and formation mechanisms of the Northern Hemisphere summertime subtropical highs, *J. Clim.*, *18*, 5046–5065.

Parkinson, C., D. Rind, R. J. Healy, and D. G. Martinson (2001), The impact of sea ice concentration accuracies on climate model simulations with the GISS GCM, *J. Clim., 14*, 2606–2623.

Peng, S., and J. S. Whitaker (1999), Mechanisms determining the atmospheric response to midlatitude SST anomalies, *J. Clim.*, *12*, 1393–1408.

Peng, S., W. A. Robinson, and S. Li (2003), Mechanisms for the NAO responses to the North Atlantic SST tripole, *J. Clim.*, *16*, 1987–2004.

Polyakov, I., et al. (2007), Observational program tracks Arctic Ocean transition to a warmer state, *Eos Trans. AGU*, *88*(40), 398.

Polyakov, I. V., et al. (2005), One more step toward a warmer Arctic, *Geophys. Res. Lett., 32*, L17605, doi:10.1029/2005GL023740.

Randall, D., J. Curry, D. Battisti, G. Flato, R. Grumbine, S. Hakkinen, D. Martinson, R. Preller, J. Walsh, and J. Weatherly (1998), Status of and outlook for large-scale modeling of atmosphere-ice-ocean interactions in the Arctic, *Bull. Am. Meteorol. Soc.*, *79*, 197–219.

Raphael, M. N. (2003), Impact of observed sea-ice concentration on the Southern Hemisphere extratropical atmospheric circulation in summer, *J. Geophys. Res.*, *108*(D22), 4687, doi:10.1029/2002JD003308.

Raymo, M. E., D. Rind, and W. F. Ruddiman (1990), Climatic effects of reduced Arctic sea ice limits in the GISS II general circulation model, *Paleoceanography*, *5*, 367–382.

Rayner, N. A., D. E. Parker, E. B. Horton, C. K. Folland, L. V. Alexander, D. P. Rowell, E. C. Kent, and A. Kaplan (2003), Global analyses of sea surface temperature, sea ice, and night marine air temperature since the late nineteenth century, *J. Geophys. Res.*, *108*(D14), 4407, doi:10.1029/2002JD002670.

Rigor, I. G., J. M. Wallace, and R. L. Colony (2002), Response of sea ice to the Arctic oscillation, *J. Clim.*, *15*(18), 2648–2668.

Rinke, A., W. Maslowski, K. Dethloff, and J. Clement (2006), Influence of sea ice on the atmosphere: A study with an Arctic atmospheric regional climate model, *J. Geophys. Res.*, *111*, D16103, doi:10.1029/2005JD006957.

Serreze, M. C., F. Carse, and R. Barry (1997), Icelandic low cyclone activity: Climatological features, linkages with the NAO, and relationships with recent changes in the Northern Hemisphere circulation, *J. Clim*., *10*, 453–464.

Serreze, M. C., A. P. Barrett, A. G. Slater, M. Steele, J. Zhang, and K. E. Trenberth (2007), The large-scale energy budget of the Arctic, *J. Geophys*. *Res.*, *112*, D11122, doi:10.1029/2006JD008230.

Sewall, J. O. (2005), Precipitation shifts over western North America as a result of declining Arctic sea ice cover: The coupled system response, *Earth Interact*., *9*, paper 26, doi:10.1175/EI171.1.

Singarayer, J. S., J. L. Bamber, and P. J. Valdes (2006), Twenty-first-century climate impacts from a declining Arctic sea ice cover, *J. Clim.*, *19*, 1109–1125.

Steele, M., W. Ermold, and J. Zhang (2008), Arctic Ocean surface warming trends over the past 100 years, *Geophys*. *Res*. *Lett.*, *35*, L02614, doi:10.1029/2007GL031651.

Stroeve J., M. M. Holland, W. Meier, T. Scambos, and M. Serreze (2007) Arctic sea ice decline: Faster than forecast, *Geophys*. *Res*. *Lett.*, *34*, L09501, doi:10.1029/2007GL029703.

Stroeve J., M. Serreze, S. Drobot, S. Gearheard, M. Holland, J. Maslanik, W. Meier, and T. Scambos (2008), Arctic sea ice extent plummets in 2007, *Eos Trans*. *AGU*, *89*(2), 13.

Ting, M., and S. Peng (1995), Dynamics of the early and middle winter atmospheric responses to northwest Atlantic SST anomalies, *J. Clim.*, *8*, 2239–2254.

Walsh, D., I. Polyakov, L. Timokhov, and E. Carmack (2007), Thermohaline structure and variability in the eastern Nansen Basin as seen from historical data, *J. Mar*. *Res.*, *65*, 685–714.

Walsh, J. E., W. L. Chapman, and T. L. Shy (1996), Recent decrease of sea level pressure in the central Arctic, *J. Clim.*, *9*, 480–486.

Wallace, J. M., Y. Zhang, and L. Bajuk (1996), Interpretation of interdecadal trends in Northern Hemisphere surface air temperature, *J. Clim., 9*, 249–259.

Zhang X., J. E. Walsh, J. Zhang, U. S. Bhatt, and M. Ikeda (2004), Climatology and interannual variability of Arctic cyclone activity: 1948–2002, *J. Clim.*, *17*, 2300–2317.

M. A. Alexander and J. Scott, NOAA Earth System Research Laboratory, Boulder, CO 80305, USA.

U. S. Bhatt, Geophysical Institute, Department of Atmospheric Sciences, University of Alaska Fairbanks, P.O. Box 75-7320, Fairbanks, AK 99775-7320, USA. (bhatt@gi.alaska.edu)

C. Deser and R. A. Tomas, National Center for Atmospheric Research, Boulder, CO 80307, USA.

J. S. Miller, ARSC, University of Alaska Fairbanks, Fairbanks, AK 99775, USA.

M. S. Timlin, Department of Atmospheric Sciences, University of Illinois at Urbana-Champaign, Urbana, IL 61801, USA.

J. E. Walsh, International Arctic Research Center, University of Alaska Fairbanks, Fairbanks, AK 99775, USA.